Available online at www.sciencedirect.com
ScienceDirect
Applied Catalysis B: Environmental 82 (2008) 244–254
APPLIED CATALYSIS B: ENVIRONMENTAL
www.elsevier.com/locate/apcatb

Oxidation pathways of malachite green by Fe^{3+}-catalyzed electro-Fenton process

Mehmet A. Oturan, Elodie Guivarch, Nihal Oturan, Ignasi Sirés *

Université Paris-Est, Laboratoire Géomatériaux et Géologie de l'Ingénieur, 5 Bd Descartes, 77454 Marne-la-Vallée Cedex 2, France

Received 9 December 2007; received in revised form 15 January 2008; accepted 24 January 2008
Available online 2 February 2008

Abstract

A very detailed scheme for the Fe^{3+}-catalyzed electro-Fenton mineralization of malachite green as a model triarylmethane dye is presented. Bulk electrolyses of 250-mL aqueous solutions of 0.5 mM malachite green with 0.2 mM Fe^{3+} as catalyst have been carried out at room temperature and pH 3.0 under constant current in an undivided cell equipped with a graphite-felt cathode and a Pt anode to assess the performance of the electro-Fenton system. *In situ* electrogeneration of Fe^{2+} and H_2O_2 from quick cathodic reduction of Fe^{3+} and dissolved O_2 (from bubbled compressed air), respectively, allows the formation of the very oxidizing species hydroxyl radical ($^{\bullet}OH$) in the medium from Fenton's reaction. A pseudo-first-order decay kinetics with an apparent rate constant of $k_{1,MG} = 0.244\ min^{-1}$ was obtained for total destruction of malachite green by action of $^{\bullet}OH$ at 200 mA, requiring 22 min for total decoloration of the solution. In the same experimental conditions, overall mineralization was reached at 540 min. Up to 15 aromatic and short-chain carboxylic acid intermediates were identified along the treatment. The evolution of current efficiency was calculated from the chemical oxygen demand (COD) removal. Based on the time course of most of the by-products and the identification of inorganic ions released, some plausible mineralization pathways are proposed and thoroughly discussed. It has been found that the electro-Fenton degradation of malachite green proceeds via parallel pathways, all of them involving primary splitting of the triaryl structure initiated by attack of $^{\bullet}OH$ on the central carbon, thus yielding two different *N*-dimethylated benzophenones. Successive cleavage of the aromatic intermediates generates oxalic acid as the ultimate short-chain carboxylic acid, whereas *N*-demethylation of some of them produces formic acid as well. Oxalic acid and its Fe^{2+} complexes, as well as formic acid, can be slowly but totally mineralized by $^{\bullet}OH$.

Keywords: Malachite green; Electro-Fenton; Mineralization pathway; Water treatment

1. Introduction

According to financial reports, the worldwide market for synthetic organic colorants is projected to increase up to $11 billion in 2008 and the production of dyestuffs is over 7×10^5 tons [1]. Synthetic dyes are used extensively by several industries, mainly in the textile dyeing process by Asian producers. It is estimated that up to 15% of the dye is lost during this operation and disposed out in the textile effluents with a remarkable spent of water [2]. From these data it is evident that the quality of water resources is being seriously threatened, from both the aesthetic and the even more worrisome toxicological standpoint [3].

Triarylmethane dyes constitute the most ancient class of synthetic dyes, but keep still their outstanding commercial position. Among them, we have selected malachite green (**1**) as a model compound to carry out an accurate investigation. This compound is a biocide widely used in aquaculture to act as an ectoparasiticide. It is also used as a food additive and coloring agent, medical disinfectant and in the dyeing process [4]. However, **1** has become highly controversial due to the risks it poses to consumers of treated fish where it has been detected [5], since it intercalates with DNA causing carcinogenesis, mutagenesis and teratogenecity [6]. Though its use has been banned in several countries, it is still being applied due to its low cost, ready availability and efficacy. The US Food and Drug Administration (FDA) has nominated **1** as a priority chemical for carcinogenicity testing [7,8].

There is growing interest in the behavior of **1** under the action of several advanced oxidation processes (AOPs). Their performance relies on the oxidation ability of the on-site

* Corresponding author. Tel.: +33 149 32 90 60; fax: +33 149 32 91 37.
E-mail address: isires@catalonia.net (I. Sirés).

0926-3373/$ – see front matter © 2008 Elsevier B.V. All rights reserved.
doi:10.1016/j.apcatb.2008.01.016

generated hydroxyl radical ($^{\bullet}OH$, $E^0(^{\bullet}OH/H_2O) = 2.80$ V vs. SHE), which is the second most strong oxidizing agent known after fluorine and leads to the conversion or combustion of organic pollutants in aqueous solution [9]. Generally, destruction of **1** by means of AOPs proceeds via two parallel pathways, either leading to its *N*-demethylation or to splitting of **1** by attack of $^{\bullet}OH$ on the central carbon, with successive cleavage of the aromatics released. Solutions containing **1** have been treated by O_3 [10], photo-Fenton under visible irradiation [11], H_2O_2 photolysis [12], sonolysis and photocatalysis with TiO_2 [13]. Chen et al. [8] proposed a mechanistic explanation in terms of carbon- or nitrogen-centered radicals for the photocatalytic treatment. Note that among these studies just a slight comment on the mineralization of **1** and the evolution of by-products is found [13].

Recently, the development of water remediation technologies with lower economical requirements is attracting a major interest. Electrochemical advanced oxidation processes (EAOPs) are a promising alternative, because they are environmentally clean and can produce larger amounts of $^{\bullet}OH$ under control of applied current. But, in contrast to AOPs, no efforts have been made to study the behavior of **1** by electrooxidation treatments. Therefore, we propose here the use of the method called electro-Fenton (EF), whose ability to destroy toxic pollutants at ambient conditions is progressively gaining the attention of many authors due to many successful results. The most spread set-up for this indirect method includes a cell where H_2O_2 is continuously produced in the polluted solution from the two-electron reduction of O_2:

$$O_{2(g)} + 2H^+ + 2e^- \rightarrow H_2O_2 \quad (1)$$

Carbon is widely used as a cathode material for H_2O_2 generation because it exhibits a wide range of electrochemical activity for O_2 reduction and low catalytic activity for H_2O_2 decomposition [14]. Thus, reaction (1) in EF process has been carried out with planar (2D) electrodes such as graphite [15] or gas-diffusion cathodes [2,16–20], as well as with tri-dimensional (3D) electrodes like reticulated vitreous carbon [21,22], activated carbon fiber [23] or carbon-felt cathodes [1,9,14,24–28]. In addition, EF requires the presence of low amounts of Fe^{2+} ions as catalyst in the contaminated acidic effluent to electrogenerate $^{\bullet}OH$ in the bulk solution from the following Fenton's reaction [17,24]:

$$Fe^{2+} + H_2O_2 \rightarrow Fe^{3+} + {}^{\bullet}OH + OH^- \quad (2)$$

Reaction (2) can be propagated in a catalytic way from Fe^{2+} regeneration, which mainly takes place by reduction of Fe^{3+} species at the cathode surface, thus avoiding the production of iron sludge [19,29–30]:

$$Fe^{3+} + e^- \rightarrow Fe^{2+} \quad (3)$$

In previous works we have examined some fundamental aspects of the Fe^{3+}/Fe^{2+} catalytic system by comparing the use of planar and tri-dimensional (3D) cathodes [9,28]. It has been concluded that the greater performance of EF with 3D cathodes can be accounted for by: (i) the *in situ* electrogeneration of Fenton's reagent from reactions (1) and (3), resulting in the promotion of organic decomposition [24], and (ii) the greater removal rate of generated carboxylic acids and their predominant Fe^{2+} complexes by $^{\bullet}OH$, in contrast to the more stable Fe^{3+} complexes [9].

This paper reports a very detailed discussion on the electrochemical oxidation pathways for the overall mineralization of acidic aqueous solutions containing malachite green (**1**) and a catalytic amount of Fe^{3+}. The experiments have been done at constant current in an undivided electrochemical cell by using a carbon-felt cathode and a Pt anode. Moreover, the great ability of this process to both destroy and mineralize **1** has been assessed from the decay kinetics of **1** and the chemical oxygen demand (COD) removal, respectively. Note that the mineralization scheme that we propose includes not only the aromatics generated following $^{\bullet}OH$ attack, but also the short-chain aliphatic carboxylic acids coming from their cleavage, as well as inorganic ions released. All compounds were detected by chromatographic techniques and the time evolution of the most significant ones was followed.

2. Experimental

2.1. Chemicals

The triarylmethane dye malachite green (**1**, $C_{23}H_{25}N_2Cl$) was reagent grade from Sigma–Aldrich and was used as received. 4-Dimethylaminobenzophenone (**4**), 4,4′-bisdimethylaminobenzophenone (**7**), 4-dimethylaminobenzoic acid (**10**), benzoic acid (**11**), 4-aminobenzoic acid (**12**), *p*-hydroxybenzoic (**14**), hydroquinone (**15**), *p*-benzoquinone (**16**), 1,2,4-benzenetriol (**17**), maleic acid (**18**), fumaric acid (**19**), glycolic acid (**20**), formic acid (**21**), oxalic acid (**22**), 4-aminophenol (**23**) and 4-nitrocatechol (**25**) were either reagent or analytical grade from Acros Organics, Fluka and Sigma–Aldrich. 3,4,5,2′,3′,4′-Hexahydroxybenzophenone and 2,2′,4,4′-tetrahydroxybenzophenone tested as possible intermediates were from Chemos GmbH and Sigma–Aldrich. Acetic and sulfuric acids, anhydrous sodium sulfate and heptahydrated ferrous sulfate as well as pentahydrated ferric sulfate used as iron ions (catalyst) sources were analytical grade from Fluka, Merck and Acros Organics. Potassium dichromate, mercuric sulfate, silver sulfate and hexahydrated ammonium iron sulfate (Mohr's salt) used for COD analysis were purchased from Riedel de Haën and Sigma–Aldrich. All solutions were prepared with ultrapure water obtained from a Millipore Milli-Q system with resistivity >18 MΩ cm at room temperature. Acetonitrile used as organic solvent for the liquid chromatography mobile phase was HPLC grade from VWR.

2.2. Apparatus and analysis procedures

Constant current electrolyses were performed with an EG&G Princeton Applied Research 273A potentiostat/galvanostat. The solution pH was measured with an Eutech Instruments CyberScan pH 1500 pH-meter. The mineralization of solutions of **1** was monitored by the removal of their

chemical oxygen demand, determined from the analytical measurements based on the potassium dichromate method (ISO 6060: 1989 standard). Samples withdrawn from the treated solution at different electrolysis times were micro-filtered onto a hydrophilic membrane (Millex-GV Millipore, pore size 0.22 mm) before analysis. COD (in mg O_2 L^{-1}) was calculated for each sample from the following relationship:

$$\mathrm{COD} = 8000 \times \frac{(V_{(\mathrm{MS})\,\mathrm{blank}} - V_{(\mathrm{MS})\,\mathrm{sample}})N_{(\mathrm{MS})}}{V_0} \quad (4)$$

where 8000 is the milliequivalent weight of oxygen (mg O_2 mol^{-1} Fe^{2+}), $V_{(MS)\ blank}$ and $V_{(MS)\ sample}$ are the volumes (in mL) of standard Mohr's salt solution used for the blank and the sample, respectively, $N_{(MS)}$ is the normality of the Mohr's salt solution (mol L^{-1}) and V_0 is the volume of the sample (mL).

The instantaneous current efficiency (ϕ, in %) at a given time t is commonly adopted to assess the efficiency of electrochemical processes in terms of electric charge. Since it is a kind of electrical or current yield with $\Delta(\mathrm{COD})_{exp}/\Delta(\mathrm{COD})_{theo}$, this parameter was then calculated from the values of the COD using the relationship [14]:

$$\phi = \frac{\mathrm{COD}_t - \mathrm{COD}_{t+\Delta t}}{I\,\Delta t}\,\frac{n}{M_{O_2}}FV \times 100 \quad (5)$$

where COD_t and $COD_{t+\Delta t}$ are the chemical oxygen demands at times t and $t + \Delta t$ (in g O_2 L^{-1}), respectively, accounting for the experimental COD abatement, and the rest of parameters yield the theoretical ΔCOD value, where I is the current (A), Δt is the electrolysis time between both COD measurements (s), n is the number of electrons transferred per mol of O_2, M_{O_2} is the molecular weight of O_2 (g mol^{-1}), F is the Faraday constant (96,487 C mol^{-1}) and V is the volume of the treated solution (L).

The decays of **1** with oxidation time and the evolution of aromatic intermediates were followed by reversed-phase HPLC chromatography using a Merck Lachrom liquid chromatograph equipped with an L-7100 pump, fitted with a Purospher RP-18, 5 μm, 25 cm × 4.6 mm (i.d.), column at 40 °C, and coupled with an L-7455 photodiode array detector selected at λ = 614 nm for **1** and at each specific maximum wavelength of UV-absorption band for aromatic intermediates. Analysis of **1** was carried out isocratically by using a 40:60 (v/v) acetonitrile/water mixture with 1% acetic acid in each solution as mobile phase, at a flow rate of 0.8 mL min^{-1}. The HPLC gradient program given in Table 1 was used for the monitoring of aromatic intermediates, at the same flow rate, to accelerate the elution of **4** and **7**. The standard solutions to prepare the external calibration curves of all aromatics were prepared in hydro-organic medium with acetonitrile to completely dissolve it. Generated short-chain carboxylic acids were identified and quantified by ion-exclusion HPLC chromatography using a Merck Lachrom liquid chromatograph equipped with an L-2130 pump, fitted with a Supelco Supelcogel H, 9 μm, 25 cm × 4.6 mm (i.d.), column at 40 °C, and coupled with an L-2400 UV detector selected at λ = 210 nm. The mobile phase was 4 mM H_2SO_4 at 0.2 mL min^{-1}. In both HPLC techniques 20-μL samples were injected into the liquid chromatograph and measurements were controlled through an EZChrom Elite 3.1 software. In all cases, identification of intermediates was made by comparison of retention times and UV spectra with those of pure standards. Verification was carried out by means of the standard addition method. NO_3^- released in treated solutions was determined by ion chromatography just injecting 25-μL aliquots into a Dionex ICS-1000 Basic Ion Chromatography System fitted with an IonPac AS4A-SC, 25 cm × 4 mm, anion-exchange column, linked to an IonPac AG4A-SC, 5 cm × 4 mm (i.d.), column guard, and coupled with a DS6 conductivity detector containing a cell heated at 35 °C under control through a Chromeleon SE software. The sensitivity of this detector was improved from electrochemical suppression using an SRS-ULTRA II self-regenerating suppressor. Measurements were conducted with a solution of 1.8 mM Na_2CO_3 and 1.7 mM $NaHCO_3$ circulating at 1.0 mL min^{-1} as mobile phase.

Table 1
HPLC elution program for the analysis of the aromatic intermediates during the treatment of malachite green solutions by electro-Fenton with carbon-felt cathode

Time (min)	Mobile phase	
	CH_3CN (%)[a]	H_2O (%)[a]
0	35	65
15	35	65
16	80	20
25	80	20
26	35	65
30	35	65

Flow rate: 0.8 mL min^{-1}.
[a] Prepared with 1% acetic acid.

2.3. Electrolytic system

Bulk electrolyses were conducted in an open, cylindrical and undivided glass cell of 6-cm diameter and 250-mL capacity. The performance of the Pt/carbon-felt cell was tested under electro-Fenton conditions, with a 4.5 cm^2 Pt cylindrical mesh as anode and a 60 cm^2 (15 cm × 4 cm) carbon-felt from Carbone-Lorraine as cathode. The anode was centered in the electrolytic cell, surrounded by the cathode, which covered the inner wall of the cell (Fig. 1). H_2O_2 was produced from reduction of O_2 dissolved in the solution, from reaction (1). Continuous saturation of this gas at atmospheric pressure was ensured by bubbling compressed air having passed through a frit at about 1 L min^{-1}, starting 10 min before electrolysis.

Stock solutions of **1** were prepared in aqueous medium by using ultra-pure water. They were filtered prior to electrolysis and their stability was ascertained by measuring their initial concentration given by comparison with HPLC calibration curves. Solutions of 250 mL containing 0.5 mM of **1** with 0.05 mM Na_2SO_4 as background electrolyte and 0.2 mM iron ions as catalyst at pH 3.0 adjusted with H_2SO_4 have been degraded at constant current (60 or 200 mA) and at room

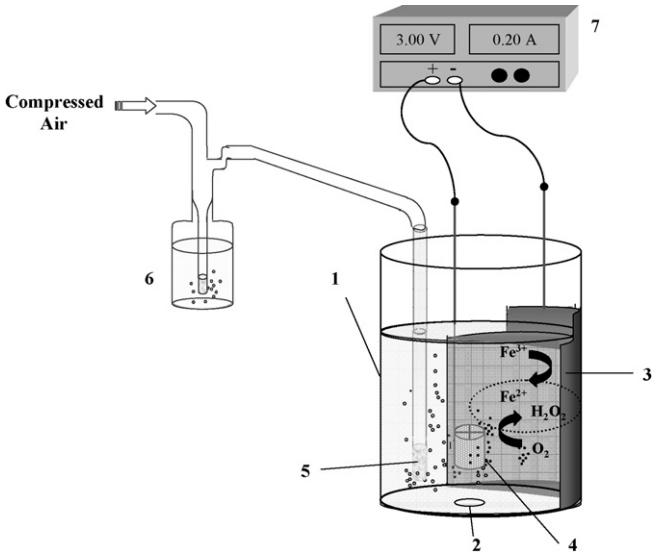

Fig. 1. Scheme of the experimental set-up used for the electro-Fenton treatments. (1) Open undivided electrolytic cell containing the treated malachite green solution, (2) magnetic stir bar, (3) carbon-felt cathode, (4) platinum anode, (5) compressed air diffuser, (6) air drying solution and (7) potentiostat–galvanostat.

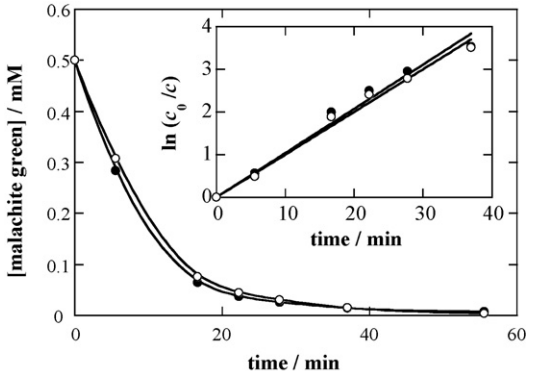

Fig. 2. Influence of the iron source used as catalyst in electro-Fenton process with carbon-felt cathode on malachite green (**1**) decay vs. electrolysis time for the treatment of 250 mL of solutions of **1** in 0.05 mM Na_2SO_4 at 60 mA, pH 3.0 and room temperature. Concentration of **1**: 0.5 mM; iron source: (●) 0.2 mM Fe^{2+}; (○) 0.2 mM Fe^{3+}. The kinetic analysis for both decay curves assuming a pseudo-first-order behavior is given in the inset panel.

temperature. The value of pH 3.0 was selected as the optimum one to carry out Fenton's reaction (2), according to several studies on electro-Fenton process [9,17]. All solutions were vigorously stirred with a magnetic bar to allow mass transfer.

3. Results and discussion

3.1. Ability of the carbon-felt cathode to continuously regenerate Fe^{2+} during electro-Fenton process

Recently, we have suggested that the fast regeneration of Fe^{2+} species at carbon-felt cathode from reaction (3) accounts for the great oxidizing power of EF system, since the existence of iron ions in the form of Fe^{2+} leads to the formation of large amounts of $^{\bullet}OH$ from Fenton's reaction (2), to the detriment of Fenton-like reactions between Fe^{3+} and H_2O_2 that generate the less oxidizing agent hydroperoxyl radical ($HO_2^{\bullet}$) [9]. Moreover, in such conditions some hardly oxidizable intermediates can form Fe^{2+} complexes that are slowly mineralized by $^{\bullet}OH$ up to be completely destroyed, as will be discussed below. In order to confirm the Fe^{2+}-regeneration ability of carbon-felt cathode that may give further support to this idea, solutions of 250 mL containing 0.5 mM of **1** and 0.05 mM Na_2SO_4 were comparatively electrolyzed at 60 mA, pH 3.0 and room temperature in the presence of 0.2 mM Fe^{2+} or Fe^{3+} as catalyst, and the decay of **1** was followed by reversed-phase HPLC chromatography, where it exhibits a well-defined peak at retention time of 13.28 min. The decay kinetics of **1**, depicted in Fig. 2, is almost the same in both cases. Malachite green is completely removed after 56 min of electrolysis, following a pseudo-first-order kinetics for its reaction with $^{\bullet}OH$, as shown in the inset. Apparent rate constants ($k_{1,MG}$) of 0.104 (square regression coefficient $R^2 = 0.989$) and 0.100 min^{-1} ($R^2 = 0.993$) were calculated for the treatments with Fe^{2+} and Fe^{3+}, respectively. This great similarity allows confirming the ability of the carbon-felt cathode to reduce Fe^{3+} species quickly from reaction (3), so in both experimental conditions Fenton's reaction produces from the beginning a high and constant concentration of $^{\bullet}OH$ in the bulk solution that follows a pseudo-first-order reaction with **1**. Note that anodic oxidation of H_2O at the anode yields a certain quantity of adsorbed hydroxyl radicals [9,19]. Results from Fig. 2 allow concluding that it is indifferent the source of iron ions selected to carry out EF process with carbon-felt cathode, so we have used Fe^{3+} for the rest of the electrolyses, since ferrous sulfate shows a lower stability towards oxidation.

3.2. Overall destruction and mineralization of malachite green aqueous solutions by EF process

It is important to study the ability of the EF system to mineralize aqueous solutions of **1**, as a previous step to the elucidation of the oxidation reaction intermediates generated. With this aim, solutions containing 0.5 mM of **1** were degraded under conditions analogous to those described in Fig. 2, with 0.2 mM Fe^{3+} and at 200 mA. A higher current was applied to shorten the total electrolysis time. First of all, the decay of **1** over time was followed as commented before to establish exactly when takes place the total decoloration of the solution. As the specific charge consumed (Q, in Ah L^{-1}) at electrolysis time t is the most usual parameter to represent mineralization data, we have used it to show in Fig. 3 the trend for the removal of **1**. Moreover, the decay has been represented as the ratio between the concentrations of **1** at time t and at zero time (c/c_0) to easily compare it with COD ratio of Fig. 4. Thus, 0.3 Ah L^{-1} are required for total decoloration of the dye solution, which is achieved when **1** is completely destroyed. The inset of Fig. 3 shows that the oxidation reaction follows a pseudo-first-order equation, but with a higher apparent rate constant ($k_{1,MG}$) of 0.244 min^{-1} ($R^2 = 0.990$) compared to that of Fig. 2 at 60 mA. In fact, the time required for total destruction at 200 mA is 22 min, what evidences a faster degradation as the applied

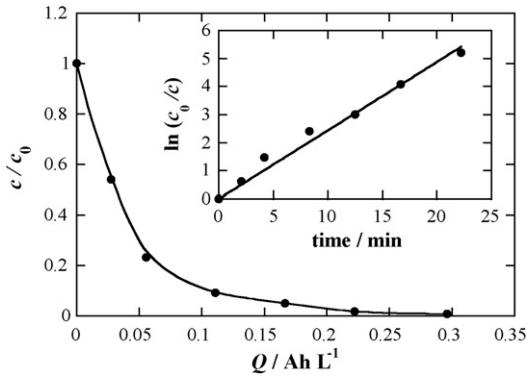

Fig. 3. Decay of malachite green vs. specific charge up to attain its overall destruction for electrolyses of 250-mL aqueous solutions containing 0.5 mM of **1**, 0.05 mM Na_2SO_4 and 0.2 mM Fe^{3+} at 200 mA, pH 3.0 and room temperature. The corresponding analysis assuming a pseudo-first-order kinetics for the oxidation of **1** by $^{\bullet}OH$ is shown in the inset by giving the trend over time.

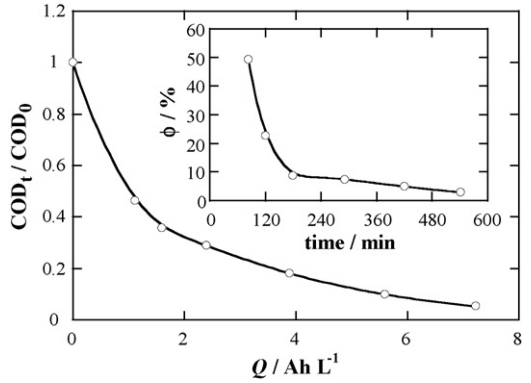

Fig. 4. COD abatement vs. specific charge for overall mineralization of **1** by electro-Fenton under operating conditions given in Fig. 3. The time evolution of the instantaneous current efficiency along the mineralization process is given in the inset panel.

current increases. This can be explained by the fact that rising current enhances the electroreduction of O_2 from reaction (1), as suggested by Brillas and co-workers [18,19], and that of Fe^{3+} from reaction (3) [29], thus yielding larger amounts of $^{\bullet}OH$ from reaction (2). Note that Chen et al. [8] reported that photodegradation of 0.14 mM of **1** with TiO_2 and UV irradiation requires up to 4 h for total destruction, so EF process seems to be an efficient treatment technique.

The decay of COD with time was analyzed for the same solutions to follow the mineralization of **1**. From the evolution of the COD ratio with Q shown in Fig. 4, it is clear that the mineralization process of **1** is much slower than its destruction, since 7.2 Ah L^{-1} (i.e., 540 min) are required to reach the overall conversion (>95% COD removal) of the initial 305.7 mg L^{-1} COD (i.e., 0.5 mM of **1**) into CO_2, H_2O and inorganic ions. This large difference can be explained by the existence of various steps throughout the treatment, as will be better clarified from the analysis of the intermediates formed. For example, just 1.2 Ah L^{-1} (i.e., 90 min) are required to decrease the COD ratio up to 0.5 (i.e., 50% COD mineralization), and 3.2 Ah L^{-1} (i.e., 240 min) are required up to 0.25. So, the mineralization process involves a long stage from 3.2 to 7.2 Ah L^{-1} entirely devoted to slowly oxidize some hardly degradable products. From Fig. 6 it will be concluded that these compounds are mainly carboxylic acids such as oxalic acid and its Fe^{2+} complexes. The instantaneous current efficiency (ϕ) was calculated from relationship (5) by using the COD values obtained from (4), and its corresponding time course is depicted in the inset of Fig. 4. Efficiency values as high as 50% are obtained at the beginning of the treatment, when the high and constant concentration of hydroxyl radicals produced can react efficiently with the great amount of initial organic matter. Thus, the compounds initially present in the solution account for a high organic matter content and, furthermore, they are relatively easy to degrade, so $^{\bullet}OH$ mainly reacts with them and leads to a high COD removal during this stage. Unfortunately, the decrease of COD along with the transformation of the aromatic intermediates into more hardly degradable compounds results in an evident fall of efficiency that leads to the progressive enhancement of quick parallel non-oxidizing reactions between $^{\bullet}OH$ and Fe^{2+} (with $k = 3.2 \times 10^8$ M^{-1} s^{-1}) or H_2O_2 (with $k = 2.7 \times 10^7$ M^{-1} s^{-1}) [9], as well as its anodic oxidation to O_2 and its recombination to produce H_2O_2. For example, ϕ is 8.8% at 180 min, and further on it slightly decreases up to the end of the process. Note that these wasting parasitic reactions, although to a lower extent, are given even at the beginning of the electrolysis, and that allows explaining the efficiency values much lower than 100% obtained at short electrolysis time. Moreover, it must be taken into consideration that $^{\bullet}OH$ is not directly generated by applying the current in the system, but it requires the diffusion of Fe^{3+} and O_2 towards the cathode and that of the reduction products Fe^{2+} and H_2O_2 towards the solution to yield $^{\bullet}OH$, which must also diffuse to react with organics in the medium.

3.3. Identification and evolution of aromatic intermediates

To study the behavior of the aromatic intermediates formed during the mineralization of **1**, solutions containing 0.5 mM of the dye were electrolyzed by electro-Fenton under the experimental conditions described in Fig. 3. It is worth noting that up to 10 aromatics could be identified along the electrolysis, what makes the elucidation of the reaction sequence to be certainly complex. Moreover, it must be remarked that none among previous studies has dealt with the evolution trends of the intermediates of **1**, so just detection has been reported.

Reversed-phase chromatograms of treated solutions, obtained with HPLC conditions mentioned in Table 1, exhibited peaks related to products summarized in Table 2, where retention times and detection wavelengths of each one are indicated. As can be seen, the 10 compounds can be distributed into four different aromatic groups: (i) benzophenones, (ii) phenols, (iii) benzoic acids and (iv) quinones.

The time course of the concentration of the two benzophenones detected, 4-dimethylaminobenzophenone (**4**) and 4,4′-bisdimethylaminobenzophenone (**7**), is shown in Fig. 5a. Also the compounds 3,4,5,2′,3′,4′-hexahydroxybenzophenone and 2,2′,4,4′-tetrahydroxybenzophenone were tested

Table 2
Classification of the aromatic intermediates identified by reversed-phase chromatography during the electro-Fenton mineralization of **1**, under the experimental conditions described in Fig. 3, regarding their functional group

Aromatic intermediates	Notation	t_R (min)	λ (nm)
Benzophenones			
4-Dimethylaminobenzophenone	**4**	19.98	352
4,4′-Bisdimethylaminobenzophenone	**7**	20.17	364
Phenols			
1,2,4-Benzenetriol	**17**	2.10	290
4-Aminophenol	**23**	2.45	270
4-Nitrocatechol	**25**	3.67	316
Benzoic acids			
4-Aminobenzoic acid	**12**	2.54	288
Benzoic acid	**11**	4.44	254
4-Dimethylaminobenzoic acid	**10**	5.55	314
Quinones			
Hydroquinone	**15**	2.39	289
p-Benzoquinone	**16**	3.40	244

Retention time (t_R) and detection wavelength (λ) are given as well.

in order to investigate the possible formation of hydroxylated benzophenones after splitting of the chromophore structure of **1**, as reported for photo-Fenton [11], but they were not found because either they are not generated in our system or they are not significantly accumulated in the medium. Comparison between data reported in Figs. 3 and 5a indicates that both **4** and **7** are formed simultaneously to **1** degradation. It is clearly seen that **4** is much more abundant than **7**, with maximum concentrations of 4.7×10^{-2} and 0.08×10^{-2} mM at 17 and 12.5 min, respectively. These values are reached precisely at a time similar to that at which **1** is totally destroyed (Q about 0.2 Ah L^{-1} in Fig. 3, corresponding to $t = 15$ min), so further on benzophenone intermediates are not formed and their concentration begins to decrease. From the amounts detected, it can be concluded that **1** tends to fragment at the bond between the central carbon atom and dimethylaminophenyl group. The concentration of **4** rapidly decreases to 0.9×10^{-2} mM at 60 min, although both **4** and **7** remain in the solution for 180–240 min because they are more slowly removed as their concentration diminish due to mass transfer limitations that make it difficult $^{\bullet}$OH attack.

The time evolution of the concentration of benzoic acids (benzoic acid (**11**), 4-aminobenzoic acid (**12**) and 4-dimethylaminobenzoic acid (**10**)) is depicted in Fig. 5b. These compounds must be generated after cleavage of the bond between the central carbon of **4** and **7** and one of the phenylic groups, thus giving rise to the carboxylic substituent. Low amounts of **10** are accumulated up to its disappearance at 120 min, whereas compound **12** appears after 30 min of electrolysis and attains a maximum concentration of 4×10^{-2} mM at about 90 min. These findings suggest that both benzophenones are transformed into **10**, which is quickly demethylated to yield compound **12**. Subsequently, **12** attains its maximum value just when concentrations of **4** and **7** are very low and **10** can be no further accumulated. Again, **12** disappears after more than 180 min due to transport limitations at final stages of its course. Regarding benzoic acid **11**, a parallel significant accumulation up to 2.5×10^{-2} mM is observed, indicating that it can be formed as an alternative to the path involving **10**.

Fig. 5c shows only the time course of phenolic compound **25** (4-nitrocatechol), because although 1,2,4-benzenetriol (**17**) and 4-aminophenol (**23**) indicated in Table 2 have been unequivocally identified, their evolution was difficult to establish correctly due to their low concentration and/or the

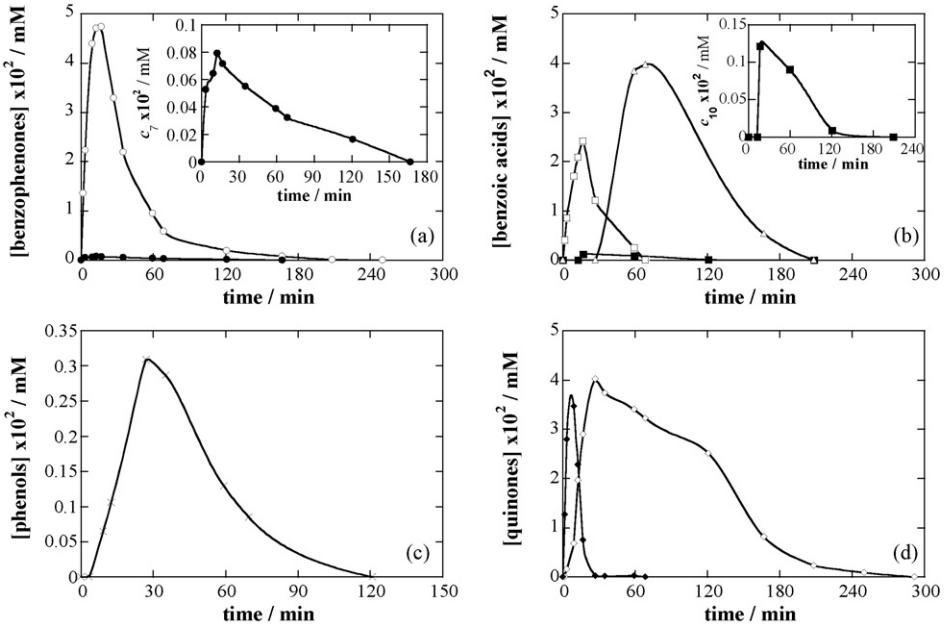

Fig. 5. Time course of the concentration of aromatic intermediates detected during the electro-Fenton mineralization of **1**, under the experimental conditions described in Fig. 3. In plot (a) benzophenones: (○) **4** and (●) **7**. A zoom for the trend of **7** is shown to clarify its evolution. In plot (b) benzoic acids: (□) **11**; (■) **10**; (Δ) **12**. A zoom for the trend of **10** is given. In plot (c) phenols: (×) **25**. In plot (d) quinones: (◇) **15** and (◆) **16**.

superposition with other peaks in such a populated zone of the chromatograms. Anyway, it can be assured that they attain values even lower than that of **25** (i.e., 0.3×10^{-2} mM at 27 min), what reveals the minor importance of the route involving phenols or their quick oxidation. 4-Dimethylbenzenamine (**5**) has also been tested, as proposed for photocatalytic and sonolytic treatment of **1** [13] but it has not been identified, probably because in case of its generation, it is quickly oxidized to its hydroxylated derivative **3** (4-dimethylaminophenol), which can be suggested as the precursor of **23**, whose low accumulation indicates its quickly conversion into **25**. Finally, **17** can be formed from hydroxylation of **25** with nitrate release.

The last group of aromatics include quinones (hydroquinone (**15**) and benzoquinone (**16**)), whose trends are represented in Fig. 5d. They achieve a maximum concentration of about 4×10^{-2} mM after 20–40 min, and later on hydroquinone is the only quinone present in the solution, remaining up to about 240 min. These two compounds constitute a redox pair, so it can be concluded that electro-Fenton with carbon-felt cathode presenting large area favors cathodic reduction of **16**. The much more slower destruction of **15** compared to the previous aromatics allows considering **15** as an oxidation intermediate formed from multiple pathways.

3.4. Identification of inorganic ions and evolution of short-chain aliphatic carboxylic acids

As pointed out above, the mineralization of **1** involves the formation of both amino and nitro aromatics, so NO_2^-, NO_3^- and NH_4^+ can be expected to be the released ions along the mineralization treatment. Thus, intermediates **12** and **23** having the $-NH_2$ group can be a source of ammonium ion, and together with **25** and other undetected compounds containing N atoms can also lead to NO_2^- and NO_3^- ions. The situation has been better clarified by electrolyzing 0.5 mM of **1** in the conditions reported in Fig. 3 and analyzing the inorganic ions accumulated in the medium by using ionic chromatography. It has been found that no nitrites are formed, whereas up to 0.85 mM NO_3^- are obtained at the end of the treatment. This amount accounts for 85% of total nitrogen content of **1** (i.e., 1 mM of N), so NH_4^+ is suggested to represent no more than 15% of initial N present in **1**. These results agree with those reported for photocatalysis and sonolysis of **1** [13]. This allows considering that whenever $^{\bullet}OH$ encounters C–NH_2 bond, the attack mostly takes place on the N atom, leading to nitroderivatives that are a source of nitrates.

The overall mineralization reaction can then be written as follows:

$$C_{23}H_{25}N_2Cl + 52H_2O \rightarrow 23CO_2 + Cl^- + 2NO_3^- + 129H^+ + 126e^- \quad (6)$$

where 126 F are required to destroy each mole of the malachite green dye.

Prolonged oxidation of aromatics weaken them and make them prone to oxidative ring opening reactions [17,24]. Ion-exclusion chromatograms of the same electrolyzed solutions showed five well-defined peaks corresponding to short-chain carboxylic acids collected in Table 3, with their retention times in the analytic conditions given in Section 2. The trends of the concentration of glycolic (**20**), formic (**21**) and oxalic (**22**) acids over time are depicted in Fig. 6, whereas maleic (**18**) and fumaric (**19**) acids were accumulated to a smaller extent (maximum values measured were about 0.02 mM). It can be seen that carboxylic intermediates are produced from the beginning of the treatment, meaning that both the formation of most of the aromatics shown in Fig. 5 and their cleavage to release carboxylics takes place from the instant at which the electrolysis starts, so mineralization of some molecules of **1** by electro-Fenton is a fast process, as evidenced in Fig. 4, where COD decrease is already initiated at zero time. Low amounts of **21** are accumulated compared to **20** and **22**, reaching its maximum value of 0.033 mM at 180 min and disappearing at 240 min. This compound could be mainly produced during the *N*-demethylation steps. This suggestion agrees with the fact that the most relevant source of **21**, i.e., compound **10** according from data of Fig. 5b, is completely destroyed at about 180–210 min, so further on acid **21** progressively disappears from the solution. Regarding glycolic acid (**20**), it is the most abundant carboxylic during the first stages, so it is supposed to be formed directly from ring opening of compounds **15**–**17**. It reaches a maximum value of 0.4 mM (30.4 mg L^{-1}) at 240 min, time at which all aromatics able to produce **20** disappear from the medium, and later on it slowly disappears up to be completely destroyed at 420 min. Finally, the evolution of oxalic acid (**22**) resembles that of **20**, because it is accumulated

Table 3
Short-chain aliphatic carboxylic acids identified by ion-exclusion chromatography at λ = 210 nm during the electro-Fenton mineralization of **1** under the experimental conditions described in Fig. 3

Carboxylic acid intermediates	Notation	t_R (min)
Oxalic acid	**22**	6.77
Maleic acid	**18**	9.00
Glycolic acid	**20**	14.16
Formic acid	**21**	15.10
Fumaric acid	**19**	16.66

Retention time (t_R) is given

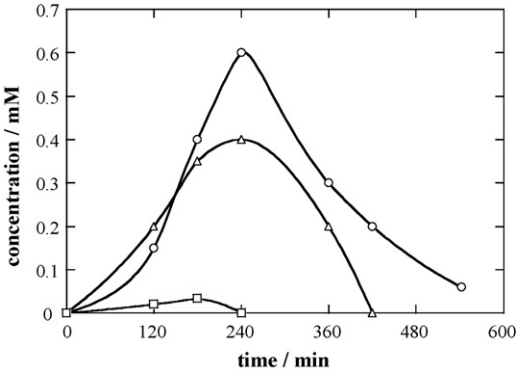

Fig. 6. Time course of the concentration of the most accumulated carboxylic acid intermediates during the electro-Fenton mineralization of **1** in the same conditions as in Fig. 3. Carboxylic acid: (Δ) **20**; (□) **21**; (○) **22**.

up to reach its maximum concentration of 0.6 mM (54 mg L^{-1}) at about 240 min, further on being removed up to its overall mineralization after 540 min. This agrees with the value of 7.2 Ah L^{-1} (i.e., 540 min) found for the Q required for overall COD depletion shown in Fig. 4. Acids **18** and **19** can be envisaged as direct precursors of **22** [19], thus justifying their very low accumulation during all the treatment, so **18**, **19** and **20** are thought to be the primary intermediates coming from the oxidative cleavage of the aryl moiety. The insignificant accumulation of **18** and **19** seems to indicate that an alternative source of acid **22** must exist to produce its high concentration. From the time course of **20**, it is plausible to propose this acid as an oxalic precursor as reported elsewhere [9], since after 240 min no aromatics remain in the solution. Therefore, oxidation of **20** up to its disappearance constantly produces a certain amount of **22**, thus delaying its destruction. In conclusion, the oxidation of carboxylic intermediates limits the mineralization of **1** and most of other aromatics compounds. The reaction between $^{\bullet}OH$ and aromatics usually presents an absolute constant rate in the range 10^8 to 10^{10} M^{-1} s^{-1} [9], whereas attack on carboxylics is much slower. For example, the absolute rate constant between $^{\bullet}OH$ and oxalic acid is 1.6×10^6 M^{-1} s^{-1} [31], what means that **22** is usually a persistent compound that determines the performance of the process. In our electro-Fenton system, both uncomplexed oxalic and Fe^{2+}–oxalate complexes can be formed, as commented in the following section, but in any case this ultimate intermediate can be finally converted to CO_2.

3.5. Mineralization pathways for the oxidative degradation of malachite green

From the large number of aromatics and aliphatic carboxylics identified along the electro-Fenton treatment of **1**, a plausible reaction sequence involving various pathways is proposed for its overall mineralization in Fig. 7. The complexity of the degradation process is caused by the multiple sites prone to $^{\bullet}OH$ attack offered by both **1** and its by-products. The species $^{\bullet}OH$ is shown as the main oxidant, although parallel action of less oxidizing agents such as O_2, $HO_2^{\bullet}$ or H_2O_2 is not discarded. Among the undetected intermediates that are included in the scheme, there are those ones that are accumulated to a small extent because they are quickly oxidized (**2**, **3**, **6**, **9**, **13**, **14**, **24** and **26**), but whose existence can be inferred from some identified products, whereas others (**5** and **8**) probably belong to minor or quicker oxidation routes. In any case, all of them appear in the figure for completeness sake.

Given the identification of *N*-dimethylated aromatic amines such as **4**, **7** and **10**, the oxidation process is initiated by hydroxylation of the central carbon of **1** to form the colorless malachite green carbinol base **2**. This was also reported for photo-Fenton treatment of **1** [11] as well as for photocatalysis of the triarylmethane dye crystal violet [32], in terms of electronic transfer between hydroxyl radical and **1**. Afterwards, four different pathways have been proposed. Paths A′ and B′ involve cleavage of different C–C bonds of central carbon along with proton abstraction to yield *N*-dimethylated benzophenones **4** and **7** along with *N*-dimethylbenzenamine (**5**) or benzene (**8**), respectively. These two latter compounds have not been detected, probably because A′ and B′ are minor routes, as previously said, or due to their quick oxidation to form hydroxylated intermediates **3** and **6**, which can be parallely generated through paths A and B that involve cleavage of the structure with simultaneous abstraction of hydroxyl radical (so-called electrophylic substitution of $^{\bullet}OH$) by monophenyl groups. Thus, the first stage of the treatment is mainly based on primary splitting of the chromophore structure by attack of $^{\bullet}OH$ on the central carbon and successive cleavage of the bond between central carbon and 4-dimethylaminophenyl or phenyl substituents, yielding benzophenones **4** and **7** plus 4-dimethylaminophenol (**3**) or phenol (**6**), respectively. The routes including these four compounds seem to be the most relevant ones, as shown in the scheme of Fig. 7, and considering the high amount of **4**, it can be conferred to path A the most outstanding role. Anyway, note that path A′ to form **4** plus **5** has been reported for the treatment by photocatalysis with TiO_2 [13,32].

The pre-eminence of path A making **1** to be splitted up into **4** and **3** was also suggested for photo-Fenton process [11] and ozonolysis [10]. On the contrary, the first ones reported a path similar to our path B, but with **1** undergoing previous *N*-demethylation to yield 4-dimethylamino-4′-aminobenzophenone.

Following the course of the major primary intermediate **4** in path A (and analogously for **4** formed in path A′), its central carbon can be hydroxylated to yield **9**, which undergoes cleavage of the bond between its central carbon and phenyl (path C′) or 4-dimethylaminophenyl (path D′) group along with proton abstraction to form **8** plus benzoic acid **10** or **5** plus benzoic acid **11**, respectively. Alternative paths C and D corresponding to hydroxyl radical abstraction are not presented because they lead to intermediates already shown (**3** and **6**), so we have preferred to simplify the scheme a bit. At this point, *N*-demethylation is proposed to quickly transform the poorly accumulated **10** into **12**, a step that was also found by Saquib and Muneer [32] during photocatalytic oxidation of crystal violet. In fact, it is well established that dimethylamino substituents are liable to be dealkylated through a radical mechanism with formation of iminium transition ion prior to amine formation. In such $^{\bullet}OH$ radical medium, methyl radicals ($^{\bullet}CH_3$) are released and, due to interaction with O_2, methyl peroxy radicals ($CH_3OO^{\bullet}$) are formed, with further decomposition to yield formaldehyde [33]. Finally, in such an oxidizing process as electro-Fenton, formic acid (**21**) can be obtained, as previously proposed from Fig. 5. Then, C–N bond of product **12** can undergo hydroxylation either on the amino group to yield nitrocompound **13** or the carbon atom to form compound **14** with loss of ammonium ion. This latter product can be parallely formed by oxidation of benzoic acids **11** and **13**, together with release of nitrate ion in the latter case. It is worth noting that product **14** has not been detected, probably due to its quick decarboxylation to yield hydroquinone **15**. Both **15** and its oxidation product **16** have been shown to be

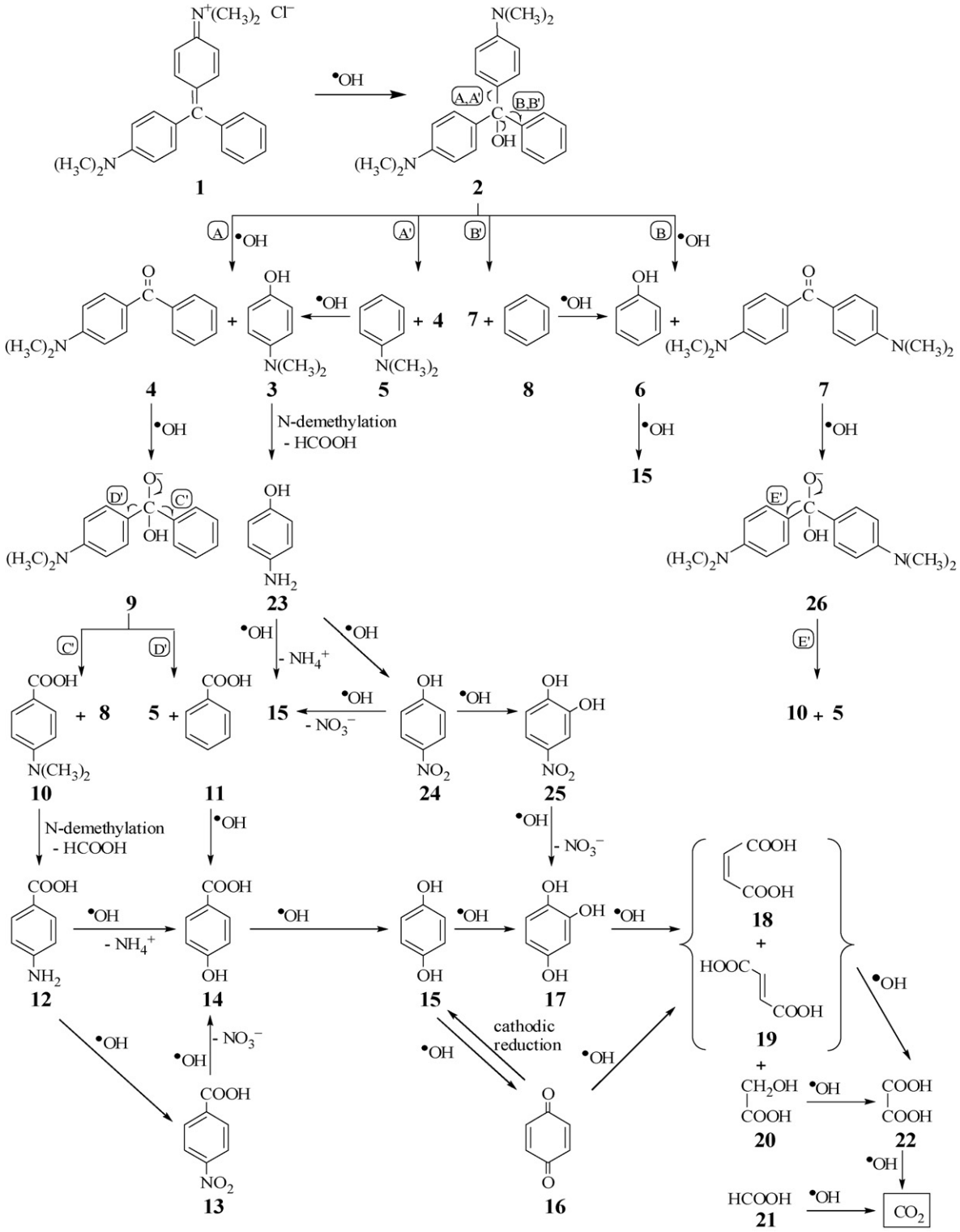

Fig. 7. Proposed oxidation pathways for malachite green (**1**) mineralization in acidic aqueous medium by electro-Fenton process with carbon-felt cathode.

important intermediates within the electro-Fenton treatment of **1**. Alternatively, •OH attack on C(2)-position of **15** leads to benzenetriol **17**, which can appear through the oxidation pathway of **3** as well. Given the existence of *N*-demethylation step transforming **10** into **12**, and based on the identification of the dealkylated product **23**, we have proposed the quick *N*-demethylation leading from the undetected compound **3** (whose standard was not available) to aminocompound **23**, with cogeneration of **21**. The proposal of *N*-dimethylated primary products **3**, **4** and **7** reinforces the idea of the triaryl structure splitting prior to *N*-demethylation processes. Next, similarly to what was explained for product **12**, C–N bond of product **23** can

undergo hydroxylation either on the amino group to yield nitrocompound **24** or the carbon atom to form **15** with loss of ammonium ion. Simultaneously, this latter product can appear from oxidation of **24**, together with release of nitrate ion. Product **24** has not been detected, probably due to its quick hydroxylation on C(2)-position, because –OH and $–NO_2$ direct the electrophile $^{\bullet}OH$ to attack ortho and meta positions, respectively, yielding **25**. $^{\bullet}OH$ attack on C(4)-position of **25** leads to benzenetriol **17** with loss of NO_3^- ion.

The appearance of path B is simpler because the fate of intermediates formed has already been discussed. Thus, attack of $^{\bullet}OH$ on phenol **6** mainly leads to **15**, whereas hydroxylation of central carbon of the minor benzophenone **7** (also formed through path B′) yields **26**, which undergoes cleavage of the bond between its central carbon and 4-dimethylaminophenyl group (path E′) along with proton abstraction to form **10** and **5**. Alternative path E corresponding to hydroxyl radical abstraction would lead to formation of **3**.

Interestingly, it must be noted that all the pathways proposed lead to the formation of **15**, a fact that allows explaining its long-time persistence observed in Fig. 5d. Further degradation of its oxidation intermediates **16** and **17** (without discarding possible opening of compound **15**, not reflected in the scheme) leads to a mixture of short-chain carboxylic acids **18**–**20**. Acid **21** formed during *N*-demethylation steps can be directly mineralized to CO_2, whereas the former three are independently converted into the ultimate carboxylic acid **22**. Acid **22** can be directly oxidized to CO_2 by hydroxyl radical at slow rate, as shown in the scheme, but it is present in the bulk solution in the form of Fe^{2+}–oxalate complexes as well [9]. Note that the formation of complexes between Fe^{2+} and other acids must also be presupposed. Therefore, the oxidation of these complexes by $^{\bullet}OH$ can be proposed according to the following reaction:

$$(Fe(C_2O_4)_n)^{(2-2n)} + 3^{\bullet}OH \rightarrow 2CO_2 + (n-1)(C_2O_4)^{2-} + Fe^{3+} + 3OH^- \quad (7)$$

where at pH 3.0, the predominant complex is given by $n = 1$. Oxalate complexes are finally oxidized to CO_2 with production of Fe^{3+}, which is quickly reduced to Fe^{2+} again, thus being able to form more Fe^{2+}–oxalate complexes as well as $^{\bullet}OH$ from reaction (2).

4. Conclusions

From the electro-Fenton treatment of aqueous solutions of malachite green as a model triarylmethane dye, it has been corroborated the great Fe^{2+}-regeneration ability of the carbon-felt cathode. This characteristic confers to the system a very remarkable oxidizing power that can be explained from the high production of a constant amount of $^{\bullet}OH$ from Fenton's reaction. The reaction of malachite green with this strong oxidizing agent leads to total decoloration of the solutions after 22 min at 200 mA, following a pseudo-first-order kinetics. The apparent rate constant increases with rising current due to the enhanced electrogeneration rate of Fenton's reagent. Overall mineralization is also obtained at 540 min, with decreasing efficiency over time leading to the progressive enhancement of parallel parasitic reactions involving $^{\bullet}OH$. The difficult oxidation of carboxylics produced from the cleavage of the aryl moiety accounts for the slow mineralization rate observed from 240 min. The large number of intermediates identified along the treatment has made it possible to propose a plausible mineralization scheme with various oxidation pathways. It has been found that destruction of malachite green by means of electro-Fenton proceeds via various parallel pathways, all of them involving primary splitting of the triaryl structure by attack of $^{\bullet}OH$ on the central carbon and successive cleavage of the aromatics released accompanied by *N*-demethylation. The ultimate by-product oxalic acid and its Fe^{2+} complexes are finally mineralized by $^{\bullet}OH$. These results allow proposing electro-Fenton process with carbon-felt cathode as an environmentally friendly method for the treatment of dye wastewaters containing malachite green.

Acknowledgment

I. Sirés acknowledges support from the Laboratoire Géomatériaux et Géologie de l'Ingénieur to obtain the ATER position in the Université Paris-Est Marne-la-Vallée.

References

[1] E. Guivarch, S. Trevin, C. Lahitte, M.A. Oturan, Environ. Chem. Lett. 1 (2003) 38–44.
[2] C. Flox, S. Ammar, C. Arias, E. Brillas, A.V. Vargas-Zavala, R. Abdelhedi, Appl. Catal. B: Environ. 67 (2006) 93–104.
[3] R.M. Christie (Ed.), Environmental Aspects of Textile Dyeing, Woodhead Publ. Ltd., Cambridge, England, 2007.
[4] S.J. Culp, F.A. Beland, J. Am. Coll. Toxicol. 15 (1996) 219–238.
[5] A.A. Bergwerff, P. Scherpenisse, J. Chromatogr. B 788 (2003) 351–359.
[6] S. Srivastava, R. Sinha, D. Roy, Aquat. Toxicol. 66 (2004) 319–329.
[7] I. Šafařík, M. Šafaříková, Water Res. 36 (2002) 196–200.
[8] C.C. Chen, C.S. Lu, Y.C. Chung, J.L. Jan, J. Hazard. Mater. 141 (2007) 520–528.
[9] I. Sirés, J.A. Garrido, R.M. Rodríguez, E. Brillas, N. Oturan, M.A. Oturan, Appl. Catal. B: Environ. 72 (2007) 382–394.
[10] M. Matsui, H. Nakabayashi, K. Shibata, Y. Takase, Bull. Chem. Soc. Jpn. 57 (1984) 3312–3316.
[11] F. Chen, J. He, J. Zhao, J.C. Yu, New J. Chem. 26 (2002) 336–341.
[12] N. Modirshahla, M.A. Behnajady, Dyes Pigments 70 (2006) 54–59.
[13] C. Berberidou, I. Poulios, N.P. Xekoukoulotakis, D. Mantzavinos, Appl. Catal. B: Environ. 74 (2007) 63–72.
[14] M. Panizza, G. Cerisola, Water Res. 35 (2001) 3987–3992.
[15] A. Da Pozzo, P. Ferrantelli, C. Merli, E. Petrucci, J. Appl. Electrochem. 35 (2005) 391–398.
[16] B. Boye, M.M. Dieng, E. Brillas, J. Electroanal. Chem. 557 (2003) 135–146.
[17] E. Brillas, B. Boye, I. Sirés, J.A. Garrido, R.M. Rodríguez, C. Arias, P.L. Cabot, C. Comninellis, Electrochim. Acta 49 (2004) 4487–4496.
[18] C. Flox, J.A. Garrido, R.M. Rodríguez, P.L. Cabot, F. Centellas, C. Arias, E. Brillas, Catal. Today 129 (2007) 29–36.
[19] I. Sirés, C. Arias, P.L. Cabot, F. Centellas, J.A. Garrido, R.M. Rodríguez, E. Brillas, Chemosphere 66 (2007) 1660–1669.
[20] G.R. Agladze, G.S. Tsurtsumia, B.I. Jung, J.S. Kim, G. Gorelishvili, J. Appl. Electrochem. 37 (2007) 985–990.
[21] C. Badellino, C.A. Rodrigues, R. Bertazzoli, J. Hazard. Mater. B137 (2006) 856–864.
[22] A. Alvarez-Gallegos, D. Pletcher, Electrochim. Acta 44 (1999) 2483–2492.

[23] A. Wang, J. Qu, J. Ru, H. Liu, J. Ge, Dyes Pigments 65 (2005) 227–233.
[24] M.A. Oturan, J. Appl. Electrochem. 30 (2000) 475–482.
[25] B. Gözmen, M.A. Oturan, N. Oturan, O. Erbatur, Environ. Sci. Technol. 37 (2003) 3716–3723.
[26] S. Hammami, N. Oturan, N. Bellakhal, M. Dachraoui, M.A. Oturan, J. Electroanal. Chem. 660 (2007) 75–84.
[27] M. Diagne, N. Oturan, M.A. Oturan, Chemosphere 66 (2007) 841–848.
[28] I. Sirés, N. Oturan, M.A. Oturan, R.M. Rodríguez, J.A. Garrido, E. Brillas, Electrochim. Acta 52 (2007) 5493–5503.
[29] Z. Qiang, J.-H. Chang, C.-P. Huang, Water Res. 37 (2003) 1308–1319.
[30] M.A. Oturan, J.L. Peiroten, P. Chartrin, A.J. Acher, Environ. Sci. Technol. 34 (2000) 3474–3479.
[31] G.U. Buxton, C.L. Greenstock, W.P. Helman, A.B. Ross, J. Phys. Chem. Ref. Data 17 (1988) 513–886.
[32] M. Saquib, M. Muneer, Dyes Pigments 56 (2003) 37–49.
[33] A.I. Cederbaum, A. Qureshi, G. Cohen, Biomed. Pharmacol. 32 (1983) 3517–3524.